J. Fluid Mech. (1989), *vol.* 206, *pp.* 1–23
Printed in Great Britain

On the stability of Kelvin waves

By W. K. MELVILLE[1], G. G. TOMASSON[1] AND D. P. RENOUARD[2]

[1] R. M. Parsons Laboratory, Massachusetts Institute of Technology, Cambridge, MA 02139, USA

[2] Institut de Mecanique de Grenoble, Saint-Martin d'Heres, France

(Received 27 July 1988 and in revised form 22 November 1988)

We consider the evolution of weakly nonlinear dispersive long waves in a rotating channel. The governing equations are derived and approximate solutions obtained for the initial data corresponding to a Kelvin wave. In consequence of the small nonlinear speed correction it is shown that weakly nonlinear Kelvin waves are unstable to a direct nonlinear resonance with the linear Poincaré modes of the channel. Numerical solutions of the governing equations are computed and found to give good agreement with the approximate analytical solutions. It is shown that the curvature of the wavefront and the decay of the leading wave amplitude along the channel are attributable to the Poincaré waves generated by the resonance. These results appear to give a qualitative explanation of the experimental results of Maxworthy (1983), and Renouard, Chabert d'Hières & Zhang (1987).

1. Introduction

The evolution of weakly nonlinear dispersive long waves in a rotating fluid has been the subject of some controversy in recent years. In the absence of rotation and weak transverse effects the subject is well developed, a result of the applicability of the Korteweg–de Vries (KdV) equation and its related equations to problems of one-dimensional propagation, with the well-known solitary-wave solutions. However, Maxworthy (1983) drew attention to the problems associated with rotation in oceanographic applications to sea straits and the continental shelves where the transverse scales of the topography are not negligible when compared to the Rossby radius. Maxworthy conducted experiments on the second-mode waves evolving from the collapse of a mixed region in a stratified fluid. The more important features of these experiments were the curvature of the wavefronts (in contrast to the corresponding straight-crested linear Kelvin waves) and their dissipation along the channel, the latter being attributed to vertical radiation of inertial waves.

In a very careful theoretical investigation Grimshaw (1985) derived evolution equations for weakly nonlinear, long internal waves in continuously stratified fluids and found that at least two cases could be separated. Strong rotation: the Rossby radius is at most comparable with the wavelength, and the effects of rotation are separable from the effects of weak nonlinearity and dispersion. The wave decays exponentially across the channel with the evolution along the channel described by a KdV equation. Weak rotation: the Rossby radius is greater than the wavelength, and the effects of rotation are not separable. The evolution equation is a rotation-modified Kadomtsev–Petviashvili (KP) equation. In no case could Grimshaw explain the wave front curvature in the absence of dissipation in a channel of finite width. He suggested that the observed curvature could be due to wave transience

associated with dissipation, or geometrical effects associated with the wave source. In the limit of infinitely wide channels he concluded that the radiation of Poincaré waves with their concomitant transverse energy flux could lead to unsteady Kelvin waves with curved crests.

Recently Renouard, Chabert d'Hières & Zhang (1987) conducted a careful set of experiments, generating first-mode internal waves in a controlled fashion on the large rotating platform at the Coriolis Laboratory, Grenoble. Their experiments showed that the decay scale across the channel was the Rossby radius (in contrast to Maxworthy) and that the amplitude at the wall decayed due to viscous dissipation. They too observed the wavefront curvature. The combination of dissipation and wavefront curvature is consistent with Grimshaw's conclusions.

Katsis & Akylas (1987) solved the rotation modified KP equation and found that the solutions they obtained were qualitatively similar to the observations of Renouard *et al.* (1987). However, there is no dissipation in the equations, so the decay along the channel wall in the numerical solutions could not be due to viscosity. They did note that the main curved disturbance was followed by smaller amplitude waves but did not relate the decay to these waves. The concluded that the weakly nonlinear inviscid theory revealed the main features observed by Renouard *et al.* (1987), and that the wavefront curvature is possible because of the attenuation along the channel.

Most recently Grimshaw & Melville (1989) have reconsidered the derivation of the rotation-modified KP equation and its integral constraints (cf. Grimshaw 1985). They concluded that, owing to the radiation of Poincaré waves behind the leading wave, in general it is not possible to assume that the solutions of the equation are locally confined.

On the basis of the work briefly reviewed above it is difficult to avoid the conclusion that weakly nonlinear Kelvin waves may be unstable, in the sense that wave solutions of permanent form do not exist†. In this paper we shall show that weakly nonlinear dispersive Kelvin waves of finite bandwidth propagating along a channel may be unstable through resonance with Poincaré waves. This is a resonance which arises due to the nonlinear correction to the speed of the Kelvin wave and may be simply shown graphically. In figure 1 we show the hydrostatic linear dispersion curves for Kelvin and Poincaré waves in a channel. We also show that a small increase in the Kelvin wave speed due to nonlinearity may lead to a direct resonance with the linear Poincaré modes.

Approximate solutions of a coupled set of evolution equations for the longitudinal and transverse velocity, which are asymptotically equivalent to the rotation-modified KP equation derived by Grimshaw (1985) and used by Katsis & Akylas (1987), are studied. These solutions display the direct nonlinear resonance and the

† Our use of the term 'unstable' requires some clarification as it departs from the common usage. Instability usually describes growing perturbations to an exact solution of the governing equations. (However in many cases the governing equations are only an approximation to the full conservation laws.) Here we *do not* establish that there exists a nonlinear Kelvin wave of permanent form for the approximate governing equations. We do show that initial disturbances which are a rational approximation to Kelvin waves of permanent form for the governing equations, and which have a null transverse velocity component, develop a growing perturbation due to interaction with other modes of the system. Consequently, the approximate unimodal solution is 'unstable'. This distinction, based on the criterion of existence of an exact solution to approximate equations, is often of little practical consequence. For example, it is well known that there exist exact permanent form solutions for nonlinear irrotational inviscid free-surface flows. However, such waves of permanent form are not physically realizable in real fluids!

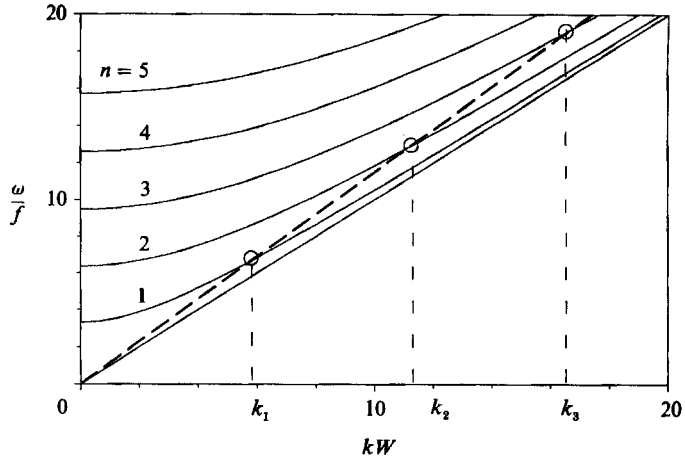

FIGURE 1. The dispersion curves for the linear hydrostatic modes of a channel (——) showing the possibility of direct resonant forcing of linear Poincaré waves by weakly nonlinear Kelvin waves (– – –) having a small positive speed correction. k_n denotes the resonant wavenumber of the nth Poincaré mode.

wavefront curvature evident in earlier laboratory and numerical experiments. The evolution equations are solved numerically, giving good agreement with the analytical solutions.

2. The coupled evolution equations

While the motivation for studying this problem comes from the dynamics of internal Kelvin waves, the elements of the problem and its resolution are to be found in the corresponding flow of a homogeneous fluid. Therefore we consider the motion of a homogeneous inviscid fluid in a rotating channel. The coupled evolution equations were originally derived in their non-rotating form by R. Winther (1985, personal communication) and subsequently by Macomb (1986) for the rotating case. All but the final steps in the derivation of the equations closely follow those of the rotation-modified KP equation which is derived in detail by Grimshaw & Melville (1989). In the interests of brevity then we shall simply introduce the scaling and quote the final equations.

We consider the motion of a homogeneous inviscid fluid in a channel of width W rotating with angular velocity $\frac{1}{2}f$ about the vertical, z-axis. The walls of the channel are parallel to the x-axis and the undisturbed depth of the fluid is h. The dimensional variables may be written

$$\left.\begin{aligned} \eta = \alpha h\eta', \quad u = \alpha c_0 u', \quad v = \alpha\gamma c_0 v', \\ t = \frac{t'}{kc_0}, \quad x = k^{-1}x', \quad y = l^{-1}y', \quad z = hz', \end{aligned}\right\} \tag{2.1}$$

where (u, v) is the first-order, depth-independent velocity vector, η is the surface displacement, α is the nonlinear parameter, c_0 is a characteristic phase speed, k^{-1} and l^{-1} are characteristic scales along and across the channel and $\gamma = l/k$. In order to introduce weak nonlinearity, dispersion, transverse variation and rotation at the same order in the evolution equations we choose

$$\alpha = \frac{a}{h}, \quad \beta = (kh)^2, \quad \Gamma = \gamma^2 = \left(\frac{l}{k}\right)^2 = \left(\frac{f}{kc_0}\right)^2, \tag{2.2}$$

such that α, β and Γ are each of the same order and much less than unity. Here a is a typical wave amplitude. This corresponds to the case of weak rotation considered by Grimshaw (1985).

Following the derivations cited above we obtain the coupled set of evolution equations for the longitudinal and transverse velocity components

$$u_t + u_x + \tfrac{3}{2}\alpha u u_x - \tfrac{1}{6}\beta u_{xxt} + \tfrac{1}{2}\Gamma[v_y - v] = 0, \tag{2.3a}$$

$$v_t + u_y + u = 0, \tag{2.3b}$$

with the boundary conditions at the channel walls

$$v = 0 \quad \text{at } y = 0, W, \tag{2.3c}$$

where to the first order we consider only waves propagating in the positive x-direction.

The linearized form of these equations has the dispersion relation

$$\omega^2[1 + \tfrac{1}{6}\beta k^2] - \omega k - \tfrac{1}{2}\Gamma[l^2 + 1] = 0, \tag{2.4}$$

where $u, v \sim \mathrm{e}^{\mathrm{i}(kx+ly-\omega t)}$. The primary root of this equation has $\omega = O(1)$ and corresponds to the linear Kelvin ($l = i$) and Poincaré modes ($l = n\pi/W, n = 1, 2, \ldots$) propagating along the channel in the positive x-direction. This root avoids the singularity at $k = 0$ in the linearized KP equation. However, a second mode given by

$$\omega = -\frac{\Gamma}{2k}[l^2 + 1] \tag{2.5}$$

exists when k scales with unity, and this corresponds to the conservation and stationarity of potential vorticity in the exact linear problem (cf. Grimshaw & Melville 1989). Hence in this formulation these wave components propagate slowly to the left unless $(l^2 + 1) = 0$, in which case they are stationary and the primary mode is the linear Kelvin wave.

3. Stability to direct nonlinear resonance

3.1. *First-order Kelvin wave solution*

We take the initial data of the system (2.3a, b, c) to correspond to a solitary Kelvin wave, with u exponentially decaying in the transverse direction and v zero everywhere. In what follows we show this wave to be unstable due to generation of Poincaré waves, thus showing that no steady solitary Kelvin wave solution exists for (2.3a, b, c).

With this choice of the initial conditions the first-order initial perturbation potential vorticity is zero, i.e.

$$q_0(x, y) = [v_x - u_y - u]_{t=0} = 0 \tag{3.1}$$

and the constraints on the initial conditions discussed by Grimshaw & Melville (1989) are satisfied.

With this in mind, we separate u into a Kelvin wave part and a Poincaré wave part, writing

$$u(x, y, t) = \bar{u}(x, t)\,\mathrm{e}^{-y} + \epsilon\tilde{u}(x, y, t) \tag{3.2}$$

and assume that $\epsilon \ll 1, \tilde{u} = O(1)$, which can be shown to hold *a posteriori* for small t by a proper choice of initial conditions.

Subsituting this expression into (2.3a) and multiplying by e^{-y} (which is an

integrating factor for v) we integrate the resulting equation over the channel width, using the boundary conditions (2.3c) to cancel terms involving v. This gives

$$(\bar{u}_t+\bar{u}_x-\tfrac{1}{6}\beta\bar{u}_{xxt})\tfrac{1}{2}(1-\mathrm{e}^{-2W})+\tfrac{3}{2}\alpha\bar{u}\bar{u}_x\tfrac{1}{3}(1-\mathrm{e}^{-3W})$$
$$+\tfrac{3}{2}\alpha\epsilon\int_0^W(\bar{u}\tilde{u})_x\mathrm{e}^{-2y}\,\mathrm{d}y+\epsilon\int_0^W(\tilde{u}_t+\tilde{u}_x+\tfrac{3}{2}\alpha\epsilon\tilde{u}\tilde{u}_x-\tfrac{1}{6}\beta\tilde{u}_{xxt})\mathrm{e}^{-y}\,\mathrm{d}y=0. \quad (3.3)$$

Anticipating the resonance mechanism described above we expect that to leading order $\tilde{u}$ will be dominated by Poincaré waves travelling at the same speed as $\bar{u}$, thus we expect $(\partial/\partial t+\partial/\partial x)\,\tilde{u}=O(\alpha)$, which is true for the first-order solution. Equation (3.3) then becomes to order (α,β)

$$\bar{u}_t+\bar{u}_x+\alpha s\bar{u}\bar{u}_x-\tfrac{1}{6}\beta\bar{u}_{xxt}=0, \quad (3.4)$$

where
$$s=\frac{\mathrm{e}^W-\mathrm{e}^{-2W}}{\mathrm{e}^W-\mathrm{e}^{-W}} \quad (3.5)$$

is a parameter describing the combined effects of nonlinearity, rotation and finite channel width on this first-order solution. (cf. Grimshaw 1985, equations (5.2) and (5.4a)).

Equation (3.4) has the solution

$$\bar{u}(x,t)=a\,\mathrm{sech}^2\left[\left(\frac{\alpha sa}{2\beta}\right)^{\frac{1}{2}}(x-ct)\right], \quad (3.6a)$$

where
$$c=1+\tfrac{1}{3}\alpha sa. \quad (3.6b)$$

Thus the leading-order solution is a solitary wave as in the non-rotating case but with a modified lengthscale and speed. This solution is the same as that found by Zhang (1986) and Grimshaw (1985) for the case of strong rotation.

3.2. *Direct resonance*

The leading-order solution is a wave of permanent form propagating with a speed c larger than the linear Kelvin wave speed and may therefore force the linear Poincaré modes of the channel at resonance as was explained in figure 1.

Combining (2.3a) and (2.3b) gives

$$v_{tt}+v_{xt}-\tfrac{1}{6}\beta v_{xxtt}+\tfrac{1}{2}\Gamma(v-v_{yy})=\tfrac{3}{2}\alpha\left(1+\frac{\partial}{\partial y}\right)[uu_x]. \quad (3.7)$$

For small t, and to the leading order, the right-hand side will be

$$\tfrac{3}{2}\alpha\left(1+\frac{\partial}{\partial y}\right)[uu_x]\approx-\tfrac{3}{2}\alpha\bar{u}\bar{u}_x\mathrm{e}^{-2y}. \quad (3.8)$$

In order to solve for v we decompose into a Fourier series in y and a Fourier integral in x, writing

$$v(x,y,t)=\sum_{n=1}^{\infty}\int_{-\infty}^{+\infty}\mathscr{V}_n(\kappa,t)\,\mathrm{e}^{\mathrm{i}\kappa(x-ct)}\,\mathrm{d}\kappa\sin\left(\frac{n\pi y}{W}\right). \quad (3.9a)$$

and
$$\bar{u}\bar{u}_x\mathrm{e}^{-2y}=-\int_{-\infty}^{+\infty}F(\kappa)\,\mathrm{e}^{\mathrm{i}\kappa(x-ct)}\,\mathrm{d}\kappa\sum_{n=1}^{\infty}b_n\sin\left(\frac{n\pi y}{W}\right), \quad (3.9b)$$

where we have chosen the sine series in y in accordance with the boundary conditions on v. Here we have accounted for the anticipated growth of $\mathscr{V}$ in time due to resonant forcing but neglected the corresponding slow decay of $\bar{u}$, and thus expect this solution to be good for small t only.

Substituting (3.9a, b) into (3.7) and solving for $\mathscr{V}_n(\kappa, t)$ using the initial conditions $v = v_t = 0$ at $t = 0$ we get

$$\mathscr{V}_n(\kappa,t) = \mathscr{F}(\kappa,n)\left[1+\frac{r_2}{r_1-r_2}\mathrm{e}^{\mathrm{i}r_1 t}+\frac{r_1}{r_2-r_1}\mathrm{e}^{\mathrm{i}r_2 t}\right] \tag{3.10a}$$

where

$$\mathscr{F}(\kappa,n) = \frac{\frac{3}{2}\alpha F(\kappa)\, b_n}{-\kappa^2c^2(1+\frac{1}{6}\beta\kappa^2)+\kappa^2 c+\frac{1}{2}\Gamma[1+(n\pi/W)^2]} \tag{3.10b}$$

and

$$r_{1,2} = \frac{\kappa}{2(1+\frac{1}{6}\beta\kappa^2)}\left([2c(1+\tfrac{1}{6}\beta\kappa^2)-1] \mp \left\{1+2\Gamma\frac{1+\frac{1}{6}\beta\kappa^2}{\kappa^2}\left[1+\left(\frac{n\pi}{W}\right)^2\right]\right\}^{\frac{1}{2}}\right). \tag{3.10c}$$

Note that $r_1 = O(\alpha)$ and $r_2 = O(1)$. Using this expression for $\mathscr{V}_n(\kappa, t)$ the full solution for $v(x, y, t)$ can be written as

$$v(x,y,t) = \sum_{n=1}^{\infty}\int_{-\infty}^{+\infty}\mathscr{F}(\kappa,n)\left[\mathrm{e}^{\mathrm{i}\kappa(x-ct)}+\frac{r_2}{r_1-r_2}\mathrm{e}^{\mathrm{i}(\kappa x-\omega_1(\kappa)t)}+\frac{r_1}{r_2-r_1}\mathrm{e}^{\mathrm{i}(\kappa x-\omega_2(\kappa)t)}\right]\mathrm{d}\kappa\sin\left(\frac{n\pi y}{W}\right). \tag{3.11}$$

Here the first term represents the forced steady-state solution, while the second and third terms represent free wave transients due to the initial conditions, with $\omega_{1,2}(\kappa)$ the frequencies of the Poincaré and potential vorticity modes described in §2.

The group velocity of the transient Poincaré modes is smaller than that of the leading wave, as can clearly be seen from the dispersion curves in figure 1. (The same applies to the potential vorticity mode, see (2.5)). As a result, with increasing time the transients will radiate away from the leading wave and the non-resonant solution will approach the steady-state solution, which is in phase with the forcing, $-\bar{u}\bar{u}_x$. However, the Poincaré waves having the same phase speed as the leading wave will be forced at resonance and thus generated continuously in time. As κ approaches the resonant wavenumber of the nth Poincaré mode (κ_n), i.e. as

$$-\kappa^2c^2(1+\tfrac{1}{6}\beta\kappa^2)+\kappa^2c+\tfrac{1}{2}\Gamma[1+(n\pi/W)^2]\to 0$$

(cf. (2.4)) we get

$$\mathscr{V}_n(\kappa,t)\to\frac{\frac{3}{2}\alpha F(\kappa_n)\, b_n}{\kappa_n[1-2c(1+\frac{1}{6}\beta\kappa_n^2)]}\left\{\frac{1}{r_2}\mathrm{e}^{\mathrm{i}r_2 t}-\frac{1}{r_2}-\mathrm{i}t\right\}, \tag{3.12}$$

where the last term represents secular growth of the Poincaré wave in time. We notice that due to the factor i, these waves will be in quadrature with the forcing.

The sine series expansion of the forcing (3.9b) induces the Gibbs phenomenon, i.e. non-uniform convergence in y with $b_n \sim n^{-1}$ for large n. Examining the solution for $\mathscr{V}_n(\kappa, t)$, from (3.10a, b) we see that away from the resonance $\mathscr{V}_n \sim b_n n^{-2} \sim n^{-3}$ for large n. As the resonance is approached we get from (3.12) $\mathscr{V}_n \to b_n/\kappa_n \sim n^{-\frac{3}{2}}$, using $\kappa_n \sim n^{\frac{1}{2}}$, which is valid for large n. Thus the sine series expansion of v (3.9a) is uniformly convergent, justifying the term-by-term differentiation used to obtain (3.10).

This analysis shows the leading-order Kelvin wave solution for u to be unstable owing to resonant forcing of the transverse velocity associated with the linear Poincaré modes of the channel. We anticipate that energy will be transferred continuously from the Kelvin wave to the Poincaré waves resulting in the decay of the first as the latter increases with time.

3.3 *Wavefront curvature*

Substituting (3.2) into (2.3*b*) we get

$$v_t + \epsilon(\tilde{u} + \tilde{u}_y) = 0. \tag{3.13}$$

Taking the initial conditions for u to satisfy (3.6*a*) (i.e. $\tilde{u} = 0$ initially), we solve for $\tilde{u}$ from (3.13) with v given by (3.9*a*) and (3.10). Writing

$$\tilde{u}(x,y,t) = \sum_{n=1}^{\infty} \int_{-\infty}^{+\infty} \left(A_n(\kappa,t) \cos\frac{n\pi y}{W} + B_n(\kappa,t) \sin\frac{n\pi y}{W} \right) e^{i\kappa(x-ct)}\, d\kappa \tag{3.14}$$

and substituting into (3.13), we solve for $A_n(\kappa,t)$ and $B_n(\kappa,t)$ to get

$$\tilde{u}(x,y,t) = \frac{1}{\epsilon} \sum_{n=1}^{\infty} \int_{-\infty}^{+\infty} \frac{n\pi/W}{1+(n\pi/W)^2} \left\{ \frac{d\mathscr{V}_n}{dt} - i\kappa c \mathscr{V}_n \right\} \left[\cos\left(\frac{n\pi y}{W}\right) - \frac{W}{n\pi} \sin\left(\frac{n\pi y}{W}\right) \right] e^{i\kappa(x-ct)}\, d\kappa, \tag{3.15}$$

with $\mathscr{V}_n(\kappa,t)$ given by (3.10). For wavenumbers away from the resonance, i.e. for

$$-\kappa^2 c^2 (1 + \tfrac{1}{6}\beta\kappa^2) + \kappa^2 c + \tfrac{1}{2}\Gamma \left[1 + \left(\frac{n\pi}{W}\right)^2 \right] = O(1),$$

we get from (3.10*a*)

$$\mathscr{V}_n(\kappa,t) = O(\alpha), \tag{3.16a}$$

$$\frac{d\mathscr{V}_n/dt}{\mathscr{V}_n} = O(\alpha), \tag{3.16b}$$

using $r_1 r_2 = O(\alpha)$, as can be seen from (3.10*c*). Thus we choose $\epsilon = O(\alpha)$ to be consistent with the assumption that $\tilde{u} = O(1)$ which was made in deriving the leading-order solution.

As we approach the resonant wavenumber, (3.12) gives

$$\mathscr{V}_n(\kappa,t) = O(\alpha)\, t, \quad \frac{d\mathscr{V}_n/dt}{\mathscr{V}_n} = \frac{1}{t}, \quad \text{for } t \geqslant 1, \tag{3.17a, b}$$

which shows that the assumption of $\tilde{u} = O(1)$ will be satisfied for $t \leqslant O(1)$ only. However, this condition on t is very restrictive since $\tilde{u}$ will only be growing linearly in time for wavenumbers close to the resonance but will remain small for all other wavenumbers. Thus we expect this analysis to be good for t somewhat larger than $O(1)$.

As t increases the dominant terms in (3.15) will be

$$\tilde{u}(x,y,t) \approx \frac{1}{\epsilon} \sum_{n=1}^{\infty} \int_{\kappa_n - \Delta\kappa}^{\kappa_n + \Delta\kappa} \frac{n\pi/W}{1+[n\pi/W]^2} (-i\kappa c \mathscr{V}_n) \left[\cos\left(\frac{n\pi y}{W}\right) - \frac{W}{n\pi} \sin\left(\frac{n\pi y}{W}\right) \right] e^{i\kappa(x-ct)}\, d\kappa, \tag{3.18}$$

i.e. only wavenumbers close to the resonance of each transverse mode will contribute.

For wavenumbers away from the resonance the solution for v approaches the steady-state solution, which is in phase with $-\bar{u}\bar{u}_x$, as discussed in §3.2. The corresponding $\tilde{u}$ is then in phase with $[\bar{u}\bar{u}_x]_t$, which is symmetrical around the crest of the leading wave. However, close to resonance the dominant terms in v are due to the secularly growing Poincaré waves, which are in quadrature with the forcing, thus the corresponding $\tilde{u}$ will be out of phase with $[\bar{u}\bar{u}_x]_t$. In figure 2 we show how this will lead to an apparent curvature of the wave front as the Poincaré waves are

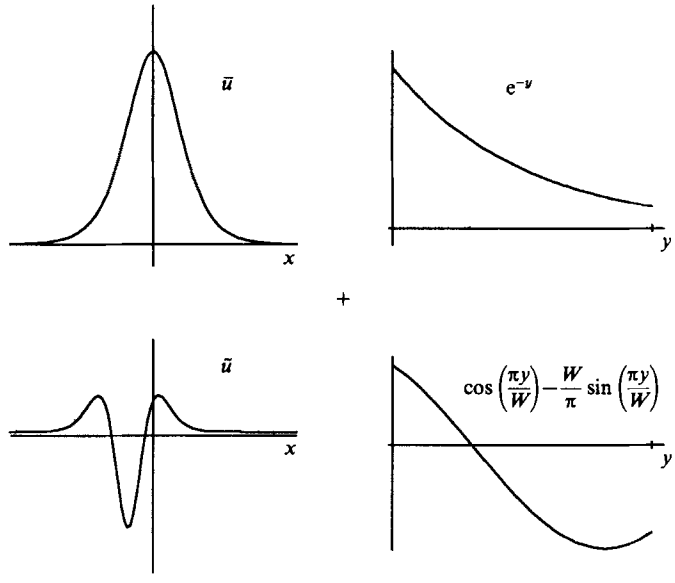

FIGURE 2. A sketch of the longitudinal and transverse structure of the leading wave and the first Poincaré mode, to explain the apparent curvature of the wavefront away from the wall as the two are added. Note that as y increases the decay of the Kelvin wave plus the longitudinal and transverse structure of the Poincaré wave lead to a curvature of the leading crest.

superposed on the leading-order wave. In this simplified example we consider only the first transverse mode (which typically dominates over the higher modes). As we move away from the right-hand wall the Poincaré wave amplitude becomes comparable with that of the Kelvin wave, leading to the backward curving of the crest away from the wall as the two are added.

Figure 3 shows an example of superposing the full solution for $\tilde{u}(x, y, t)$ on the straight-crested leading wave, $\bar{u}(x, t)\,\mathrm{e}^{-y}$, using parameters typical of the numerical solutions given in §4. Here $\bar{u}(x, t)$ is calculated according to (3.6*a*, *b*) and $\tilde{u}(x, y, t)$ is calculated from (3.15), using $\mathscr{V}_n(\kappa, t)$ as given by (3.10*a*, *b*, *c*). The resulting wave has a wavecrest curved backwards away from the wall, in good qualitative agreement with experiments and numerical solutions to be introduced in §4.

The shape of the curved wavecrest is very sensitive to changes in the phase of $\tilde{u}$. A direct comparison of these approximate solutions with numerical solutions showed small phase differences in $\tilde{u}$ leading to a slightly wider and flatter wavecrest in the approximate solutions than in the numerical solutions. These differences were attributed to the small but cumulative effect of our assumption of constant leading wave speed (cf. figure 8).

4. Numerical solutions

4.1. *Wave evolution*

Before solving (2.3*a*, *b*) numerically, we renormalize using the scaling

$$x = (\tfrac{1}{6}\beta)^{\frac{1}{2}}x', \quad y = y', \quad t = (\tfrac{1}{6}\beta)^{\frac{1}{2}}t', \quad u = \frac{2}{3\alpha}u', \quad v = \tfrac{4}{3}\sqrt{6}\frac{1}{\alpha\Gamma\beta^{\frac{1}{2}}}v', \tag{4.1}$$

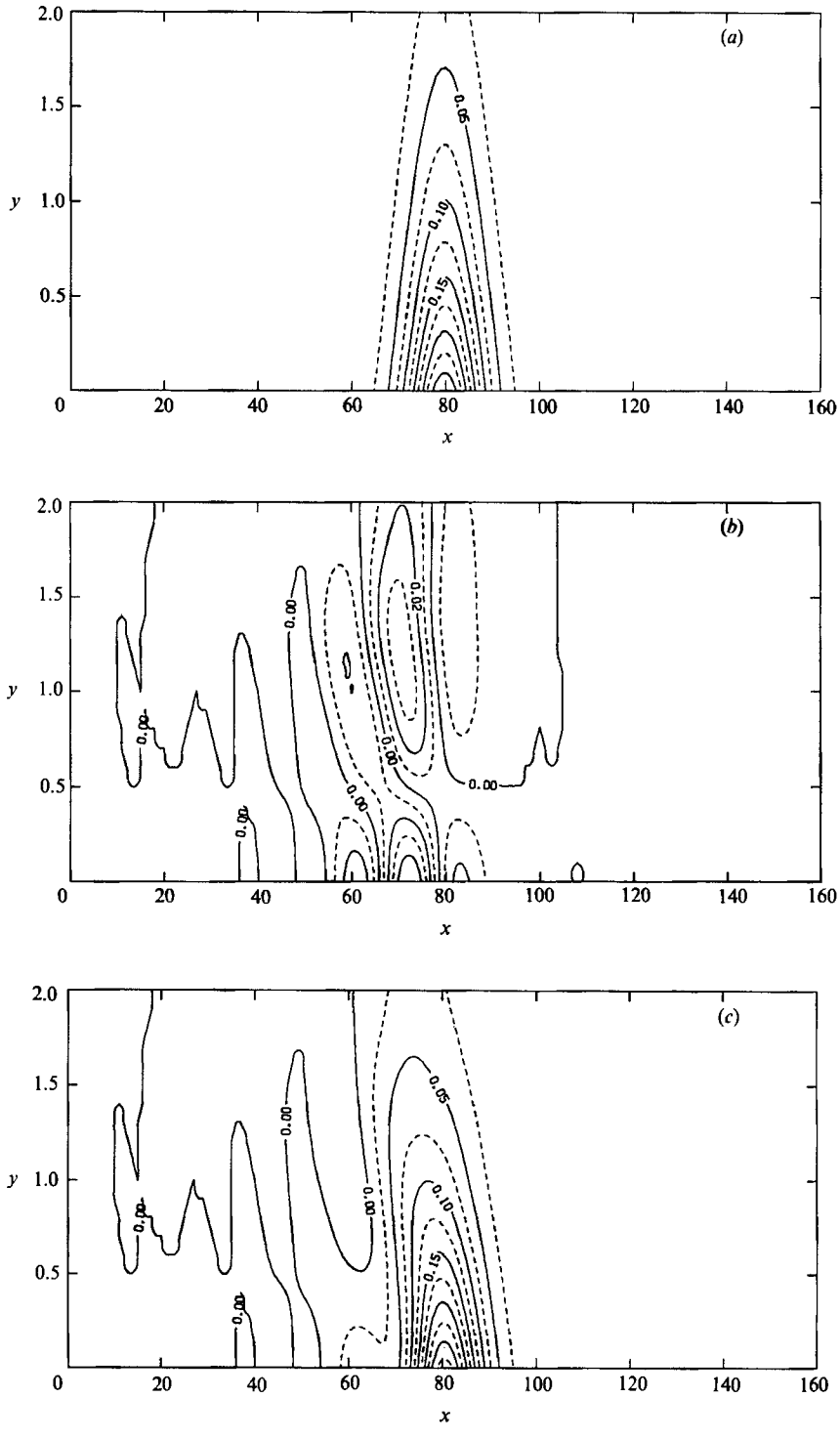

FIGURE 3. Contour maps of a typical analytical solution for u, showing the apparent curvature of the wave as the Poincaré modes are superposed on the straight-crested Kelvin wave. This and subsequent figures employ the units defined by (4.1) unless otherwise stated. (*a*) $\bar{u}(x,t)\,\mathrm{e}^{-y}$ with $\bar{u}$ given by (3.6*a*, *b*); (*b*) $\tilde{u}(x,y,t)$ calculated from (3.15); (*c*) $u(x,y,t) = \bar{u}(x,t)\,\mathrm{e}^{-y} + \tilde{u}(x,y,t)$.

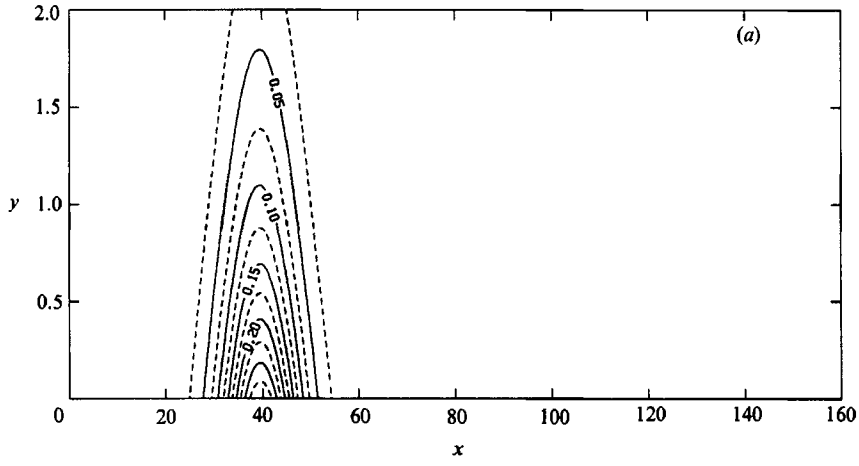

FIGURE 4(a). For caption see facing page.

where primes denote the new non-dimensional variables. This gives the equations

$$u_t + u_x + uu_x - u_{xxt} + v_y - v = 0, \tag{4.2a}$$

$$v_t + \gamma(u + u_y) = 0, \tag{4.2b}$$

with boundary conditions

$$v(x, 0, t) = v(x, W, t) = 0, \tag{4.3a}$$

$$u(0, y, t) = u(L, y, t) = 0, \tag{4.3b}$$

where L is the length of the channel used in the numerical solutions. Initial conditions are as described in §3:

$$u(x, y, 0) = a\,\mathrm{sech}^2\left[\left(\frac{sa}{18}\right)^{\frac{1}{2}}(x - x_0)\right]\mathrm{e}^{-y}, \tag{4.4a}$$

$$v(x, y, 0) = 0. \tag{4.4b}$$

Here $\gamma = \frac{1}{12}\Gamma\beta$ and the primes have been dropped for convenience.

Using the finite-difference, staggered-mesh scheme, as proposed by Winther (1985) and described by Macomb & Melville (1987), we obtain second-order accuracy in both space and time. Here we present detailed results from one run with $R/W = 0.5$. Results from runs with different rotation rates ($R/W = 1.0$ and 2.0) were consistent with this case. We take $h/W = 0.05$ and $L/W = 10$, where R, W, h, L are the dimensional Rossby radius, width, depth and length of the channel, respectively. In this run $a = 0.3$, $\Delta x = 0.25$ and $\Delta y = \Delta t = 0.1$.

In figures 4 and 5 contour plots of the solutions for u and v are shown at four different times. Consistent with the experimental and numerical results described in §1 we see a solitary wave with a crest curved backwards, followed by a train of smaller amplitude waves. We notice that the transverse structure of v is dominated by the first transverse mode, especially in the leading wave. This feature was even more evident in runs with lower rotation rates.

Figure 6 shows the decay of the amplitude of u across the channel, both normal to the wall (from the point of the maximum amplitude at the wall), and along the crest of the wave. This is compared to the linear Kelvin wave decay at two different times. For the large time the decay normal to the wall is close to the linear decay, while the decay along the crest is considerably slower; this was even more evident for slower

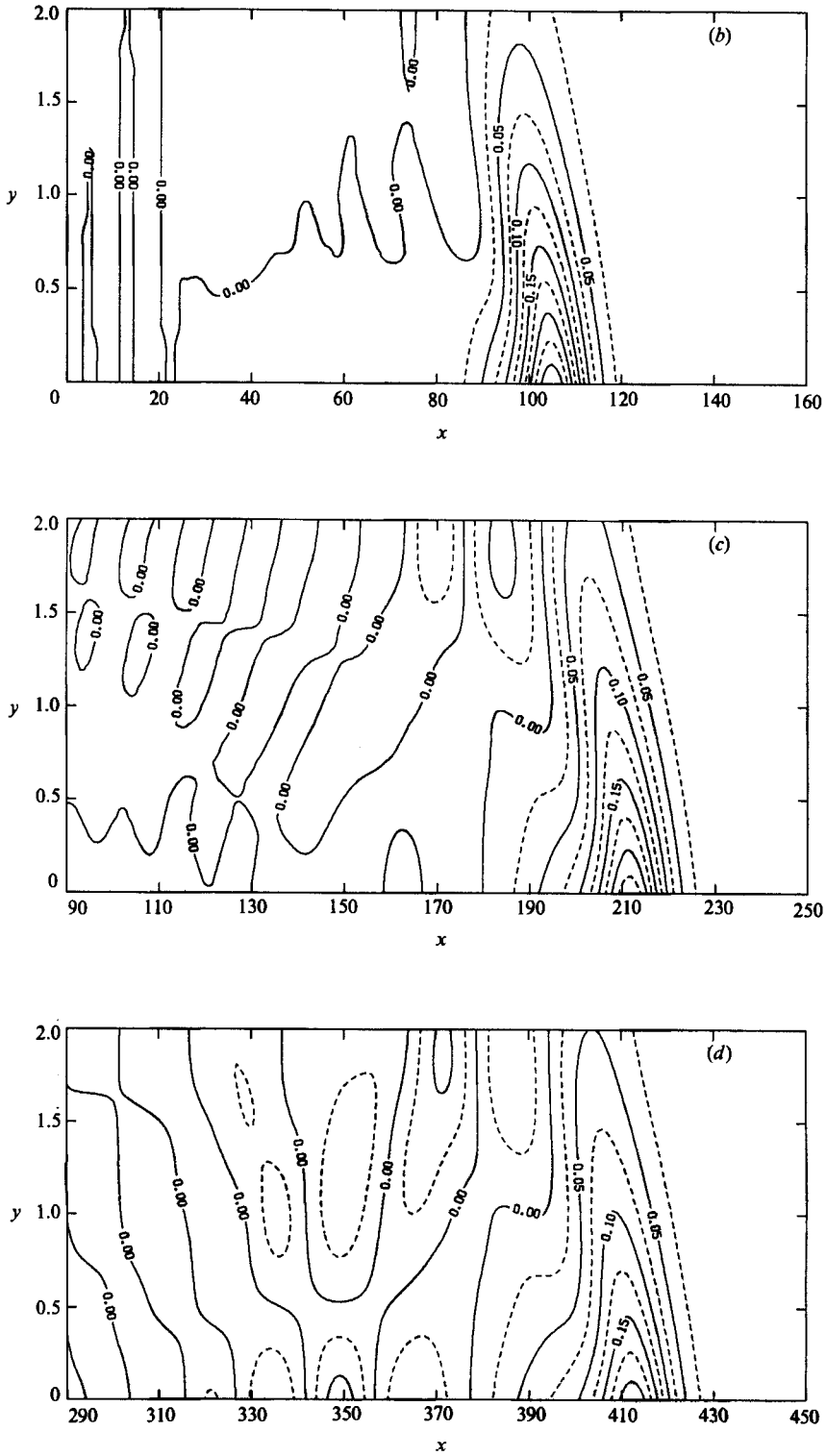

FIGURE 4. Contour maps of the solution for u with $R/W = 0.5$ at four different times. (*a*) $t = 0$; (*b*) 60; (*c*) 160; (*d*) 350.

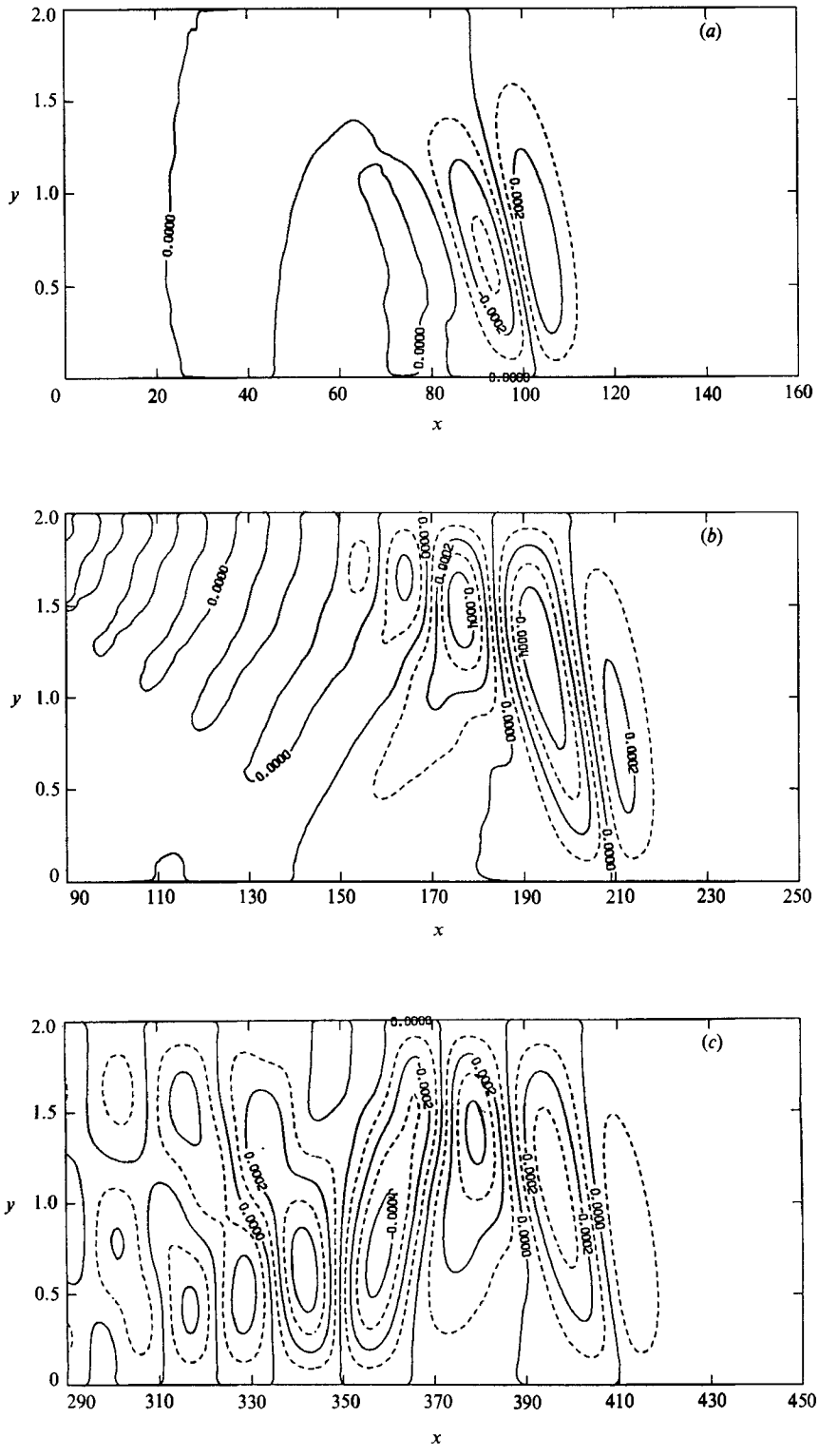

FIGURE 5. Contour maps of the solution for v at the same times as given in figure 4 for u, except the initial conditions are not shown ($v = 0$ initially). (*a*) $t = 60$; (*b*) 160; (*c*) 350.

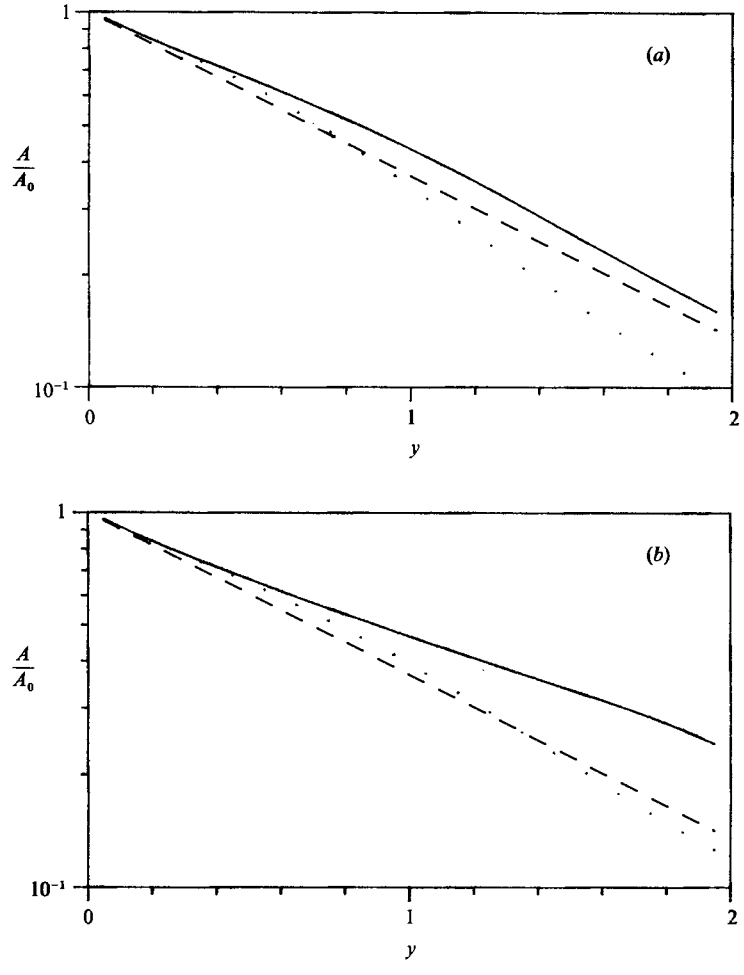

FIGURE 6. The decay of the amplitude of the leading wave across the channel, both normal to the wall from the point of maximum amplitude at the wall (·····), and along the wavecrest (——). Also shown is the linear Kelvin wave decay (– – –). (*a*) $t = 60$; (*b*) 350.

rotation rates. This can be attributed to the superposition of the forced Poincaré waves on the Kelvin wave: as we move away from the wall the Poincaré wave amplitude becomes comparable with the Kelvin wave amplitude (cf. figure 3 and §3).

The maximum amplitude of the leading wave at the right-hand wall is shown in figure 7 as a function of time for three different rotation rates. Again this is in qualitative agreement with the experimental results described in §1, and in the absence of viscous damping the leading wave decays in amplitude as it propagates down the channel. The decay depends on the rotation rate. For the slowest rotation rate the amplitude increases far down the channel. Again, this can be attributed to the superposition of the forced Poincaré waves on the leading-order Kelvin wave.

Finally, in figure 8 we show the location of the leading wavecrest at the wall versus time, the slope of this line giving the propagation speed. This is shown for $R/W = 0.5$ only; for lower rotation rates the speed increases slightly, consistent with (3.6*b*). For comparison we have also plotted lines corresponding to a constant speed of propagation for the initial conditions using equation (3.6*b*), and for the linear wave

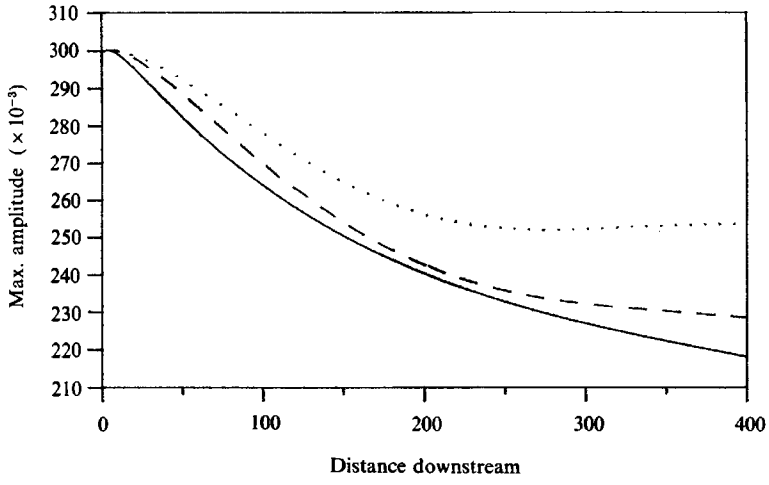

FIGURE 7. The attenuation of the maximum amplitude of the wave at the right-hand wall versus distance along the channel, shown here for three different rotation rates: ——, $R/W = 0.5$; – – –, 1.0; ·····, 2.0.

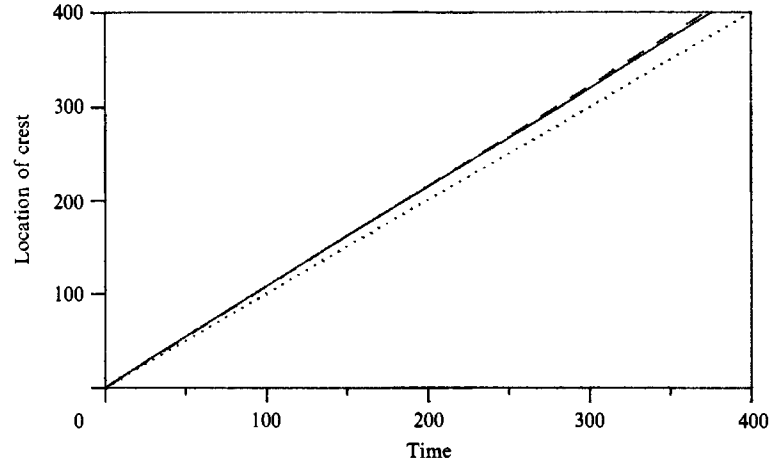

FIGURE 8. Position of the maximum of the leading wave at the right-hand wall versus time. ——, measured from the numerical solutions (note the slight decrease in speed with time); – – –, the constant nonlinear speed predicted from the initial conditions by (3.6*b*); ····, the linear wave speed.

speed. We notice that the computed speed decreases slightly with time, owing to the decreasing amplitude of the leading wave, again consistent with (3.6*b*).

4.2. *Resonant forcing of Poincaré waves*

In figure 9 the longitudinal wavenumber spectra of the first three transverse modes of v are shown at four different times. The spectra are obtained from the numerical solutions for v by first taking the Fourier-sine transform in y and then Fourier transforming each transverse mode in x, using a standard FFT algorithm. As time increases the resonant forcing of v is evident with the bandwidth of the spectra decreasing and the peaks tuning to the predicted resonant wavenumbers. In table 1

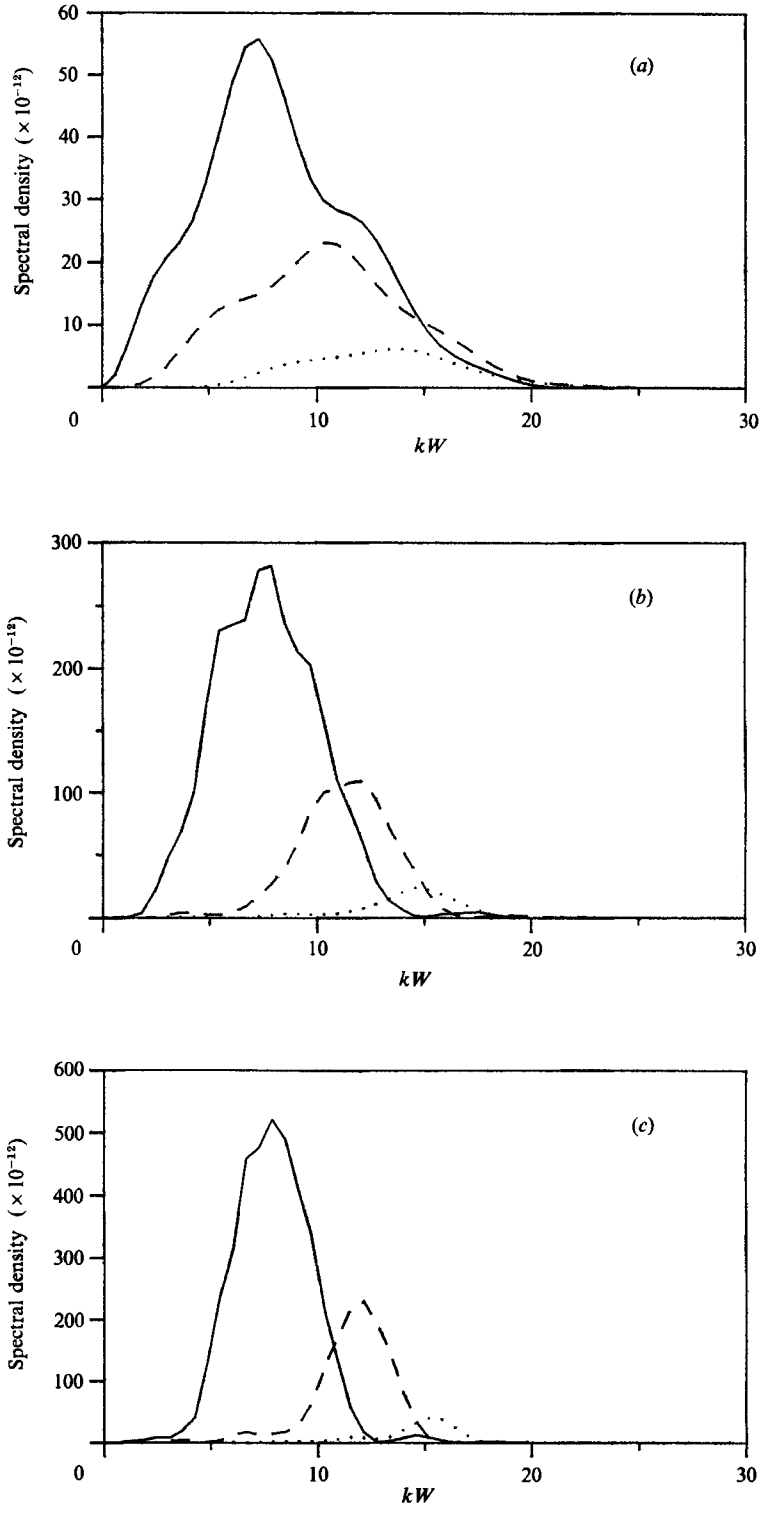

FIGURE 9(*a–c*). For caption see next page.

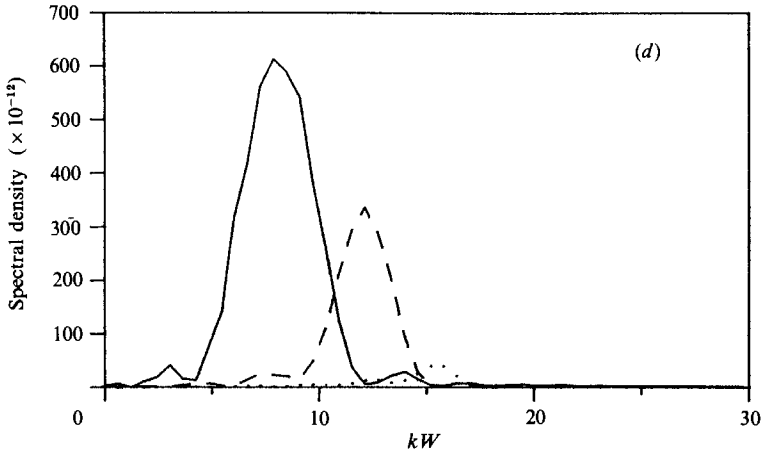

FIGURE 9. The longitudinal wavenumber spectra of the first three transverse modes of v, obtained from the solution for v by first taking the Fourier-sine transform in y and then Fourier transforming each mode in x: ——, $n = 1$; – – –, 2; ·····, 3. (*a*) $t = 60$, (*b*)160, (*c*) 250, (*d*) 350. (Note that in this and subsequent figures k is scaled by W^{-1}, whereas in the governing equations separate longitudinal and transverse lengthscales are employed.)

		Computed kW			
n	Predicted kW	$t = 60$	$t = 160$	$t = 250$	$t = 350$
1	8.2	7.1	7.6	8.0	8.1
2	12.3	10.6	11.7	12.0	12.2
3	15.7	13.8	14.6	15.4	15.6

TABLE 1. Resonant wavenumbers predicted from initial data and the wavenumbers of the peaks of the computed spectra of v

the observed wavenumbers of the peaks are compared to the predicted resonant wavenumbers. The agreement between predicted and observed values is very good, especially as t increases.

In figures 10 and 11 we compare the computed growth of individual components of v to the solution given by (3.10). This is done for the first two transverse modes and two different longitudinal wavenumbers: one close to the resonant wavenumber of the first mode, and the other close to the resonant wavenumber of the second mode. Recall that owing to the slowly changing nonlinear wavespeed the exact resonance wavenumber is not well defined. Again, the agreement is very good, especially for small t.

Finally in figure 12 we compare the predicted spectra of individual transverse modes at a given time against corresponding spectra from the numerical solutions. This is done for $t = 120$ and the agreement is good; however, as time increases we expect increasing errors, as can be seen from figures 10 and 11.

Thus we conclude that the analysis given in §3 quantitatively describes the evolution of the numerical solutions, i.e. the leading-order Kelvin wave is unstable owing to resonant forcing of the linear Poincaré waves.

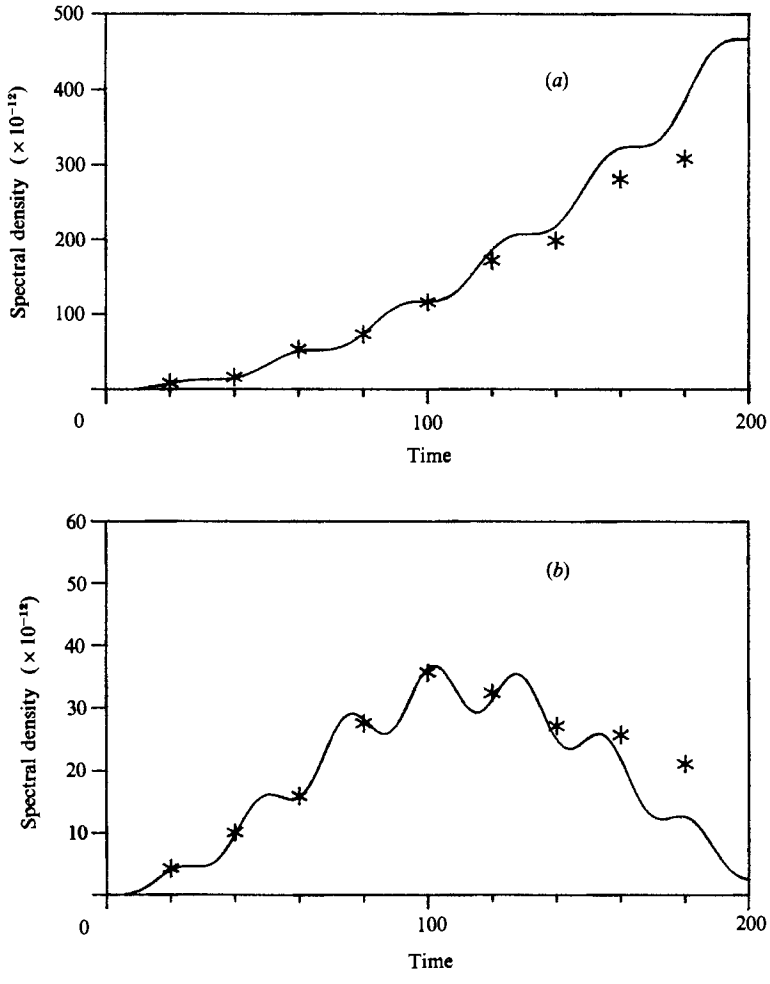

FIGURE 10. Growth of individual Fourier components of v as predicted by (3.10*a*, *b*, *c*) (——), and computed (*), for the first two transverse modes at $kW = 8.0$ (close to the resonance of the first transverse mode). (*a*) First transverse mode; (*b*) second transverse mode.

4.3. *Wavefront curvature*

From the numerical solution for v we can compute $\tilde{u}$ from (3.15) and subtract this from u to give the first-order solution. In figures 13 and 14 we show contour plots of $\tilde{u}$ and $u-\tilde{u}$ at two different times, using only the first three transverse modes for v and $\tilde{u}$.

In the solution for $\tilde{u}$, as well as v, the Poincaré wave structure is evident (cf. Gill 1982, figure 10.2). As t increases the Poincaré wave wake increases in length owing to the lower group velocity of the Poincaré waves compared with the leading-order Kelvin wave (as may be seen from the dispersion relationship in figure 1). Subtracting $\tilde{u}$ from u gives a straight-crested wave consistent with the analysis in §3.

To check the shape of the profile we compare the wavelength of $\bar{u}$ at the wall (λ) (defined as twice the distance between the point of the maximum amplitude and the point ahead of the crest where the amplitude is half the maximum amplitude) to the

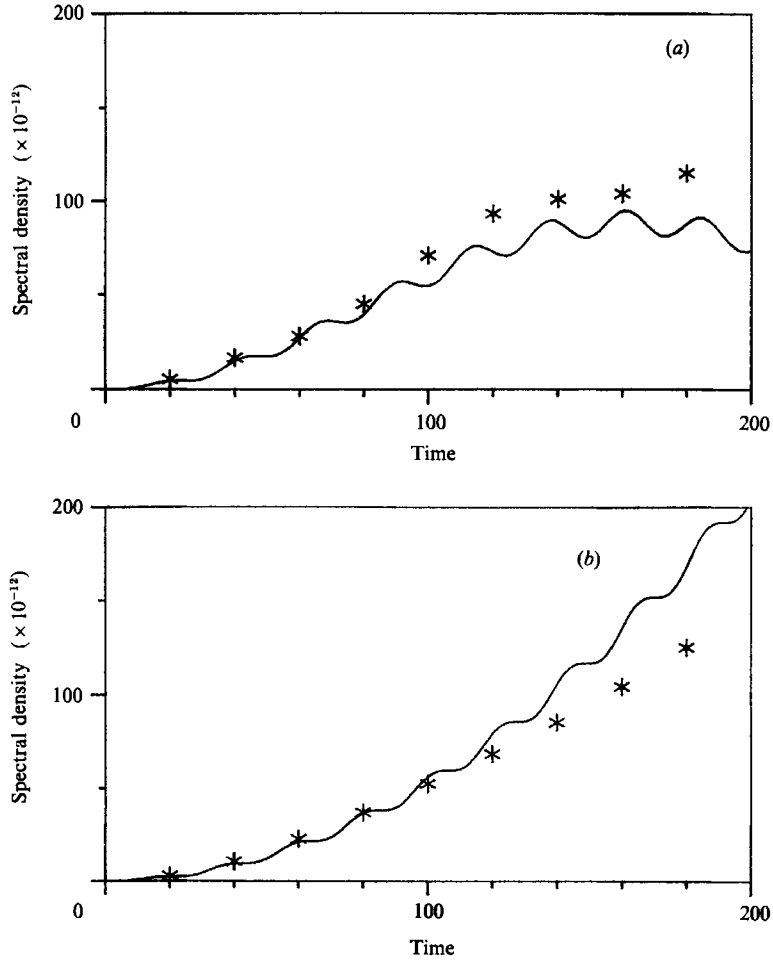

FIGURE 11. Same as figure 10, except $kW = 12.0$ (close to the resonance of the second transverse mode). (*a*) First transverse mode; (*b*) second transverse mode.

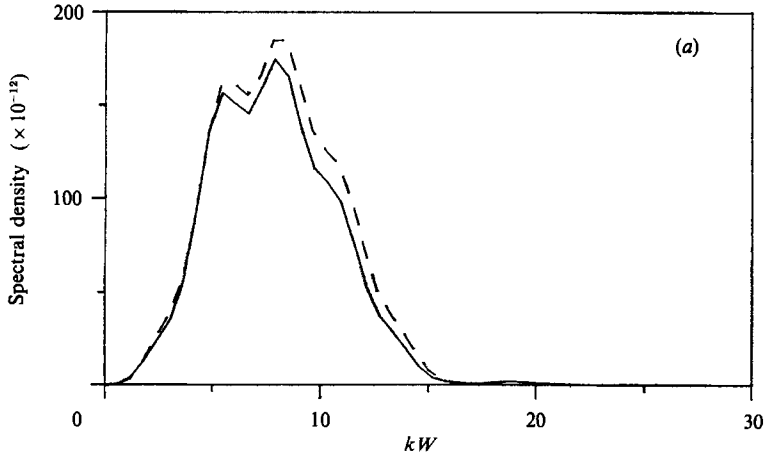

FIGURE 12(*a*). For caption see facing page.

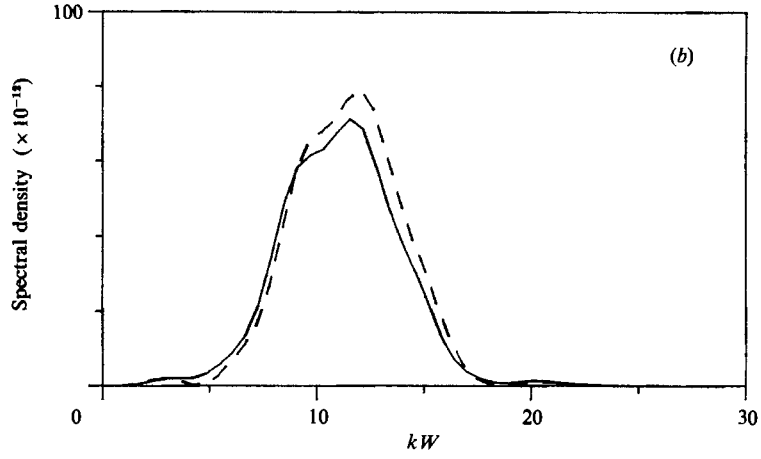

FIGURE 12. Longitudinal wavenumber spectra of individual transverse modes of v predicted by (3.10a, b, c) (– – –), and computed (——), at $t = 120$. (a) First transverse mode; (b) second transverse mode.

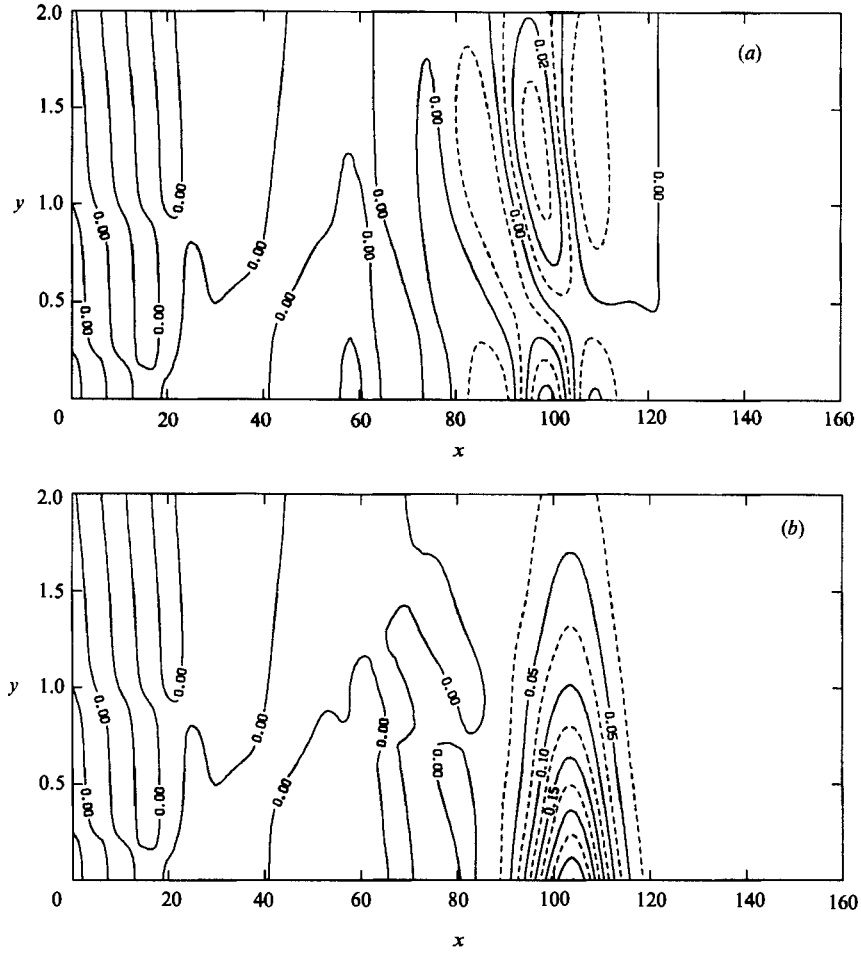

FIGURE 13. Contour maps of the solutions for (a) $\tilde{u}$ and (b) $(u-\tilde{u})$ at $t = 60$. $\tilde{u}$ is calculated from (3.15) using the numerical solution for v.

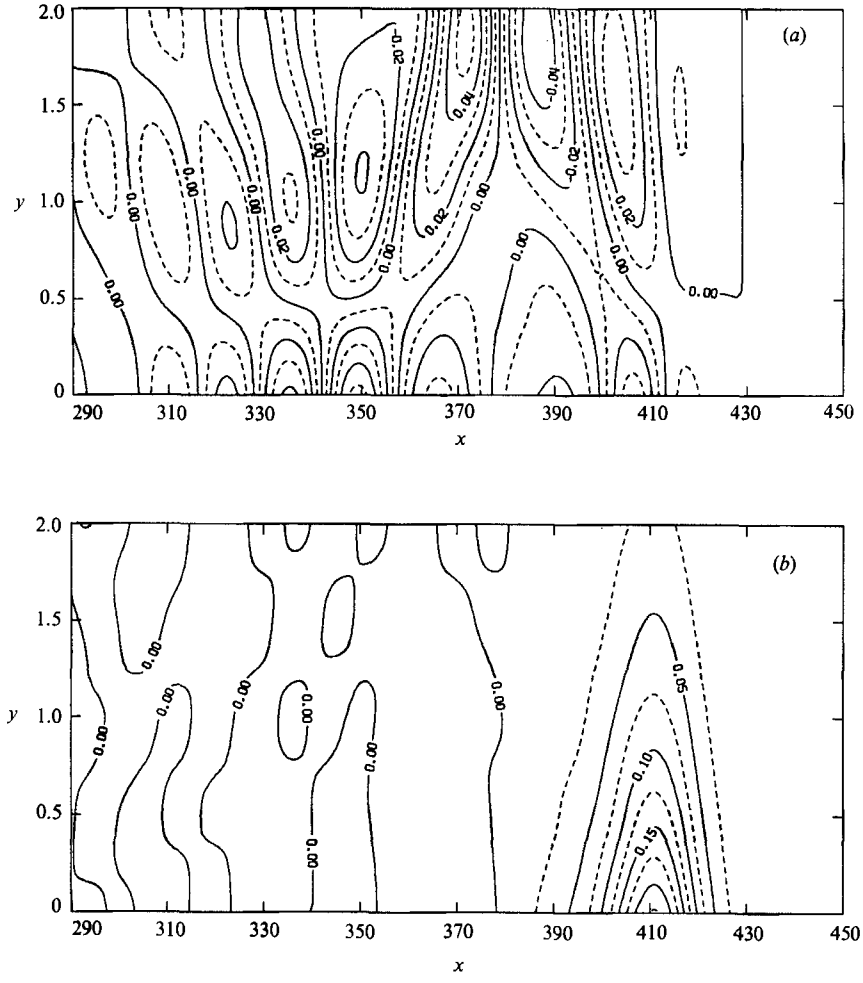

FIGURE 14. Same as figure 13 except $t = 350$.

wavelength predicted by (3.6a). In figure 15 we plot λ^{-1} *vs.* $a^{\frac{1}{2}}$, where a is the amplitude at the wall. The agreement is good.

In figure 16 we plot the speed correction as measured from the numerical solutions against the amplitude at the wall and compare to the predicted relationship from (3.6b). The agreement is fairly good; the difference can be attributed to difficulties in estimating the small nonlinear speed correction from the numerical solutions, due to the discreteness of the solutions.

5. Discussion

For reasons of simplicity and exposition we have considered the stability of barotropic Kelvin waves although as stated earlier the original motivation for this work came from the baroclinic problem. It may be shown (Tomasson 1988) that there is a complete equivalence between the single-layer case treated here and a corresponding two-layer flow. It is of interest then to ask whether the instability we have examined is likely to occur in natural flows. To this end we have taken

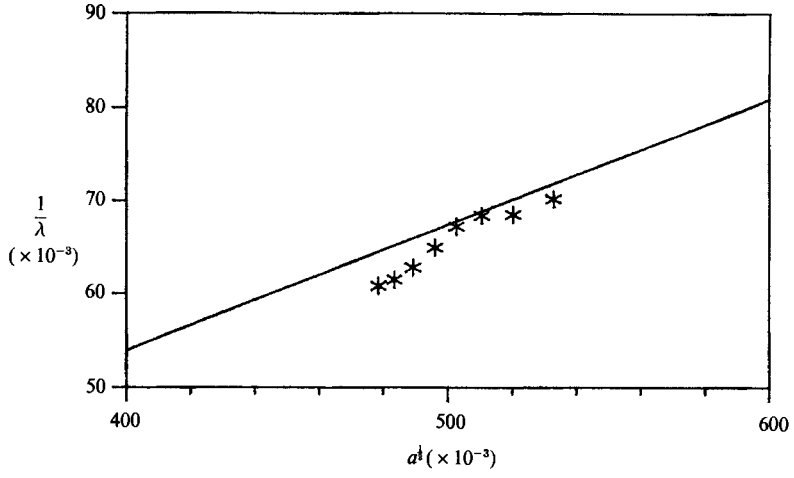

FIGURE 15. The wavelength of the leading-order wave, λ, predicted by (3.6*a*) (——), and computed for $u-\bar{u}$ (*).

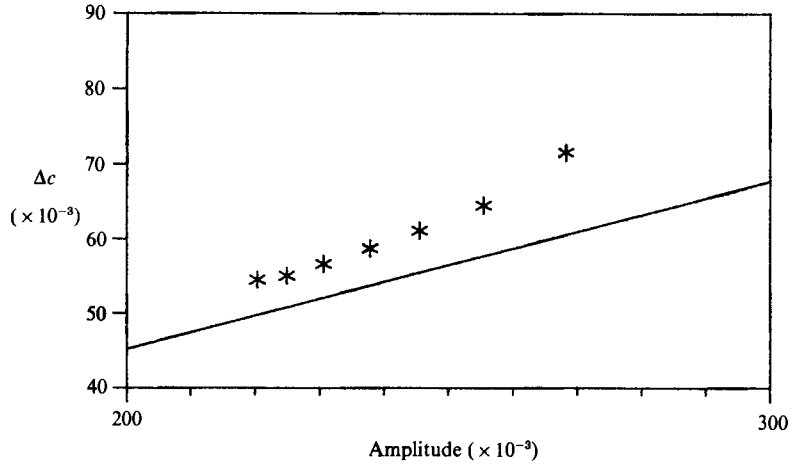

FIGURE 16. The nonlinear speed correction predicted by (3.6*b*) (——), and derived from the numerical solutions (*).

parameter values appropriate to a two-layer model of the Strait of Gibraltar, as presented in table 2.

These data have been used to generate figure 17, which shows the dispersion curves for the hydrostatic baroclinic Kelvin wave and the first five Poincaré modes for the channel. We see that the nonlinearity is sufficiently strong to excite Poincaré waves whose length along the Strait is comparable with the width of the Strait. This would remain so even if the nonlinearity were reduced by a factor of two or three. The parameters for the Strait of Gibraltar then are comparable with those in the numerical solutions presented in §4, and thus we expect that the resonance described here may be observable.

Of course, no naturally occurring strait has homogeneous boundaries and the reference state is usually not quiescent, involving both baroclinic and barotropic flows. In this case waves of the kind studied here may evolve upstream of

Upper layer depth, h_1	100 m
Lower layer depth, h_2	400 m
Normalized density difference, $\Delta\rho/\rho$	0.002
Linear phase speed, $c_0 = \left(g\frac{\Delta\rho}{\rho}\frac{h_1 h_2}{h_1+h_2}\right)^{\frac{1}{2}}$	1.25 m s^{-1}
Rossby radius, c_0/f	15 km
Approximate channel width, W	20 km
Approximate channel length, L	40–80 km
Wave amplitude, a	40 m
Nonlinear speed, $c = c_0\left[1+\frac{1}{2}\frac{\lvert h_1-h_2\rvert}{h_1 h_2}a\tfrac{2}{3}s\right]$	$1.11c_0$
$s = \frac{e^W - e^{-2W}}{e^W - e^{-W}}$	1.15

TABLE 2. Parameters estimated for a two-layer model of the Strait of Gibraltar

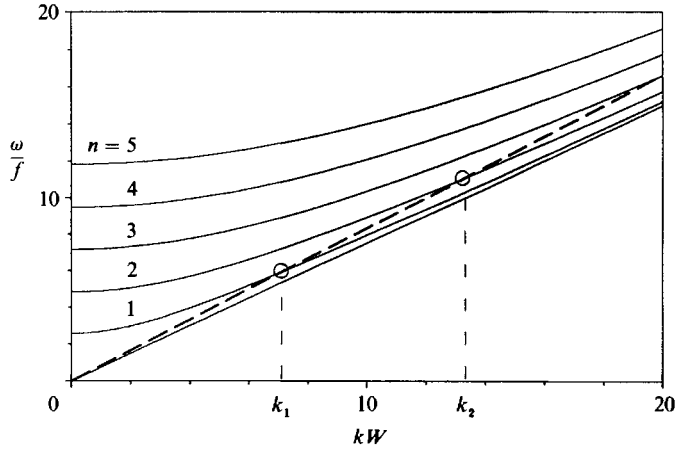

FIGURE 17. The dispersion curves for the hyrostatic baroclinic Kelvin wave and the first five Poincaré modes of a channel, together with the nonlinear Kelvin wave, using parameters estimated for the Strait of Gibraltar.

constrictions (or inhomogeneities) in the strait when the flow speed is close to the linear Kelvin wave speed as shown by Melville, Renouard & Zhang (1988).

The senior author wishes to acknowledge the support and hospitality of the University of Grenoble and CNRS, and the award of a John Simon Guggenheim Fellowship. This research was also supported by ONR (Coastal Sciences).

REFERENCES

ARMI, L. & FARMER, D. 1984 The internal hydraulics of the Strait of Gibraltar and associated sills and narrows. *Oceanol. Acta* **8**, 37–46.

GILL, A. E. 1982 *Atmosphere–Ocean Dynamics*. Academic.

GRIMSHAW, R. 1985 Evolution equations for weakly nonlinear, long internal waves in a rotating fluid. *Stud. Appl. Maths* **73**, 1–33.

GRIMSHAW, R. & MELVILLE, W. K. 1989 On the derivation of the modified Kadomtsev–Petviashvili equation. *Stud. App. Maths* (In press).

KATSIS, C. & AKYLAS, T. R. 1987 Solitary internal waves in a rotating channel: A numerical study. *Phys. Fluids* **30**, 297–301.

MACOMB, E. S. 1986 The interaction of nonlinear waves and currents with coastal topography. M.S. thesis, Department of Civil Engineering, MIT.

MACOMB, E. S. & MELVILLE, W. K. 1987 On the generation of long nonlinear waves in a channel. Unpublished manuscript.

MAXWORTHY, T. 1983 Experiments on solitary internal Kelvin waves. *J. Fluid Mech.* **129**, 365–383.

MELVILLE, W. K., RENOUARD, D. & ZHANG, X. 1988 On the generation of nonlinear internal Kelvin waves in a rotating channel. *J. Phys. Oceanogr.* (*Sub judice*).

RENOUARD, D. P., CHABERT D'HIÈRES, G. & ZHANG, X. 1987 An experimental study of strongly nonlinear waves in a rotating system. *J. Fluid Mech.* **177**, 381–394.

TOMASSON, G. G. 1988 On the stability of long nonlinear Kelvin waves. M.S. thesis, Department of Civil Engineering, MIT.

WHITHAM, G. B. 1974 *Linear and nonlinear waves*. Wiley.

WINTHER, R. 1985 Model equations for long, almost plane waves in nonlinear dispersive systems. Unpublished manuscript.

ZHANG, X. 1986 Conbtribution a l'étude des ondes internes non linéaires en présence d'une topographie ou de rotation. Doctoral thesis, University of Grenoble.